

## P1.16 IMPROVED TOA BROADBAND SHORTWAVE AND LONGWAVE FLUXES DERIVED FROM SATELLITES OVER THE TROPICAL WESTERN PACIFIC

Mandana M. Khaiyer\*, Michele L. Nordeen, Rabindra Palikonda, David. A. Rutan, Yuhong Yi  
Science Systems and Applications, Inc, Hampton, VA

Patrick Minnis and David R. Doelling  
Atmospheric Sciences, NASA-Langley Research Center, Hampton, VA

### 1. INTRODUCTION

Satellites are a valuable means for monitoring the radiation budget that drives the Earth's climate. They can be used to measure top-of-atmosphere (TOA) broadband (BB) shortwave (SW) and longwave (LW) fluxes over large portions of the Earth. The VISST (Visible Infrared Solar Split-Window Technique) satellite retrieval algorithm facilitates derivation of these parameters from various satellites, including the Geostationary Operational Environmental Satellites (GOES) and Multifunctional Transport Satellites (MTSAT). However, only narrowband (NB) fluxes are available from these satellites, so deriving BB fluxes requires use of narrowband-to-broadband (NB-BB) conversion coefficients. In a recent study, NB-BB conversion fits were derived using the NB fluxes from VISST/GOES data along with BB fluxes observed by the CERES (Clouds and the Earth's Radiant Energy Budget; Wielicki et al, 1998) instrument aboard *Terra*, a sun-synchronous polar-orbiting satellite that crosses the equator at 10:30 local time (Khaiyer et al., 2009). That effort focused on the Atmospheric Radiation Measurement (ARM) Program's Southern Great Plains (SGP) covering 32°-42°N, 91°-105°W. This study expands on that focus by deriving NB-BB coefficients for the ARM Tropical Western Pacific (TWP) Darwin region. Previous NB-BB fits typically employed in the derivation of TWP BB fluxes were based on data from other satellites and regions and may not be representative of the TWP. Thus, this study represents a significant step forward in deriving more accurate TWP BB fluxes.

To ensure accuracy in the derived BB fluxes, LW and SW NB-BB fits are separated by ocean and land, as well as by season. In the TWP region, the dry season runs from May to October, and the wet season from November through April. Validation of the BB fluxes derived from these improved NB-BB fits is performed using BB fluxes from CERES *Aqua*, as well as BB fluxes derived using the Fu and Liou (1993) radiation code.

### 2. METHODOLOGY

The VISST is used to process GOES-9 and MTSAT1-R data with a nominal pixel resolution of 4 km. The VISST (Minnis et al., 2010), which employs radiances from 0.65, 3.9, 11 and 12- $\mu$ m channels to retrieve cloud and radiative properties, facilitates the derivation of the TOA NB fluxes (from 11  $\mu$ m brightness

temperature) and albedos (from 0.65  $\mu$ m radiances). NB-BB coefficients are then derived by regressing GOES NB fluxes against the BB fluxes retrieved from radiances measured by the CERES scanner on *Terra*.

The CERES BB SW and LW fluxes are provided per each footprint (20 km at nadir for Terra) by the Single Scanner Footprint, TOA and Surface Flux, Clouds product (SSF; Geier et al, 1999). CERES further grids these SSF footprint data into a 1° gridded average product, the Monthly Gridded Single Satellite TOA and Surface Fluxes and Clouds (SFC) product. The CERES SFC cross-track mode fluxes are matched to VISST (GOES or MTSAT) 1° gridded NB fluxes within a 15 minute window, for viewing zenith angles of less than 65° (CERES) and 70° (VISST). Anisotropy within the radiance-to-flux conversion is accounted for by employing CERES ADMs (Angular Distribution Models), which vary based on cloud and scene type (Loeb et al, 2003). The ADMs take into account 6 land scene types as well as a number of cloud variables including cloud fraction, phase, and optical depth.

From the matched GOES NB and CERES BB fluxes, the following empirical equations are developed to convert NB flux to BB:

$$SWM_{bb} = a_0 + a_1 * S_{nb} + a_2 * S_{nb}^2 + a_3 * \ln(1/csza), \quad (1)$$

where  $SWM_{bb}$  is the SW BB flux,  $S_{nb}$  is the SW NB flux,  $csza = \cos(SZA)$ , and SZA is the solar zenith angle.

$$OLR_{bb} = A_0 + A_1 * L_{nb} + A_2 * L_{nb}^2 + A_3 * L_{nb} * \ln(colRH) \quad (2)$$

where  $OLR_{bb}$  is the LW BB flux,  $L_{nb}$  is the LW NB flux, and  $colRH$  is the column-weighted relative humidity RH.

VISST retrievals of GOES-9 data were made from May 2003 – October 2005, using European Center for Medium-Range Weather Forecasting/ Data Assimilation Office (ECMWF/DAO) results to provide vertical profiles of temperature and humidity. The VISST-derived NB and CERES-observed BB fluxes are used to derive coefficients for the TWP region surrounding Darwin, covering 0°-17°S, 121°E-140°E. Five sets of seasonal coefficients for LW and SW NB-BB fits are derived employing the VISST and CERES data: dry (May-October), and wet (November-April), further separated by land and ocean, within the 2.5 year period. To improve the diurnal variability in the LW NB-BB fits, separate fits are derived for daytime and nighttime. A similar procedure was followed for 1 set of preliminary fits for MTSAT Oct-Dec07.

The BB fluxes derived in this way are then evaluated using the Fu-Liou radiation transfer model, a correlated-

---

Corresponding author: Mandana Khaiyer, Science Systems and Applications, Inc, 1 Enterprise Pkwy, Suite 200, Hampton, VA; E-mail: m.m.khaiyer@nasa.gov

k, delta-two stream (2 for SW, 2/4 for LW) model. Fluxes were derived using this model for a 1° region inland near Darwin. Spectral surface emissivities for the 12 Fu-Liou bands were provided by Wilber et al (1999). Inputs for the model were provided from different sources; the aerosol optical depths were derived from Multi-Filter Rotating Shadowband Radiometer (MFRSR) data. Surface albedo for a 1° box (centered on 13.5°S 130.5°E) was provided from monthly mean CERES/SARB (Surface and Atmospheric Radiation Budget) maps (Rutan et al, 2009). Soundings and skin temperature were taken from ECMWF/DAO analyses.

### 3. RESULTS

Figure 1 shows a regression of GOES NB albedos derived over the TWP Darwin region (0°-17°S, 121°E-140°E) versus *Terra* CERES BB albedos over (a) land during November 2003–April 2004 (wet season) and (b) ocean during May-October 2004 (dry season). For 1,836 cases, the average land Wet03 season CERES BB albedo is 0.2188, with an average GOES NB albedo of 0.2132; the regression RMS error is 6.8%.

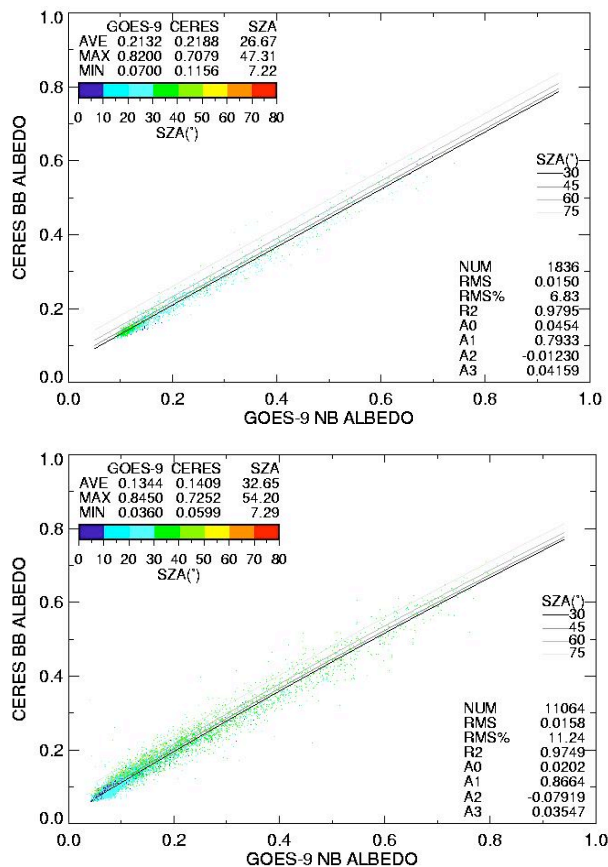


**Fig.1** Regression of SW NB GOES and Terra CERES BB fluxes over the Darwin region of the TWP (0°-17°S,121°E-140°E), for a) land wet season (Nov03-Apr04) and b) ocean dry season (May-Oct03). The NB-BB coefficients (Ax) are listed at plots' lower right.

The 11,064 ocean Dry04 cases yield an average CERES albedo of 0.1409, versus a GOES NB albedo of 0.1344; the regression RMS error is higher than that, 11.2%, for Wet03 land. The regression coefficients (Ax) listed at plots' lower right can be used to convert narrowband fluxes to broadband, using equation (1) for SW. Regressions were also performed for the remaining dry and wet seasons through May03-October05 (not shown).

Figure 2 shows similar regression fits to those in Fig. 1, but created using October-December 2007 MTSAT NB and CERES Terra BB albedos. Although the MTSAT NB-BB fits were derived separately for land and ocean, the data for MTSAT were not separated by season as for GOES9. Thus, this set of fits is considered preliminary. The domain covered is the same as that used for the GOES9 fits, and shows SW scatterplots for (a) land and (b) ocean. For 1,636 land cases, the average CERES BB albedo is 0.2094 vs 0.2352 for MTSAT, with an RMS error of 8.9%. For 5,841 cases, the average ocean CERES BB albedo is 0.1637 compared to the MTSAT NB albedo of 0.1715; the regression RMS error is 15.9%. The RMS errors for each season and satellite are summarized in Table 1.

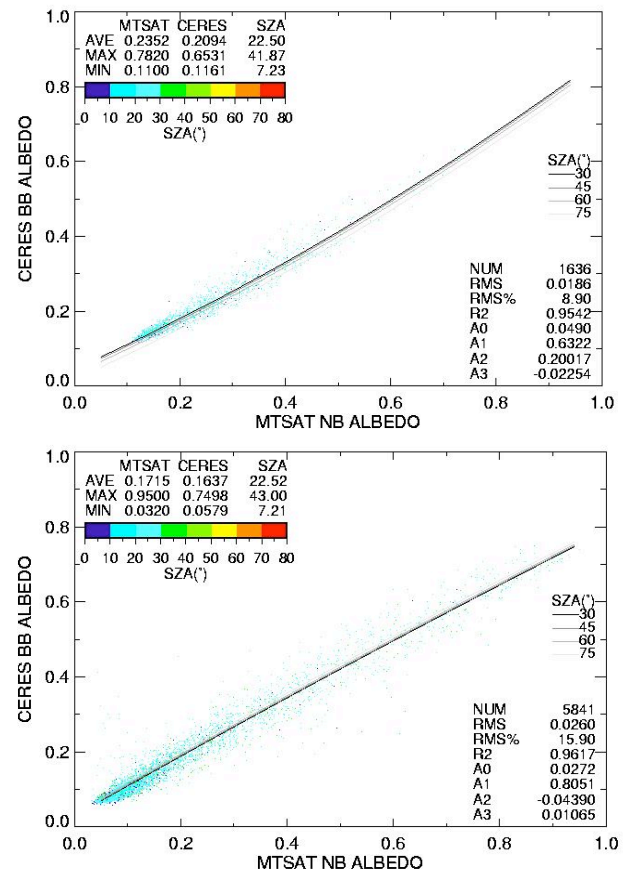


**Fig.2** Regression of SW NB MTSAT and Terra CERES BB fluxes for same region as in Fig.1, for Oct-Dec07 a) land and b) ocean. The NB-BB coefficients (Ax) are listed at plots' lower right.

**Table 1.** RMS errors in  $W/m^2$  (LW) and percent (as indicated) for GOES9 and MTSAT vs CERES *Terra* NB-BB fits, separated by seasons, day vs night, land vs ocean, for both LW and SW. D=Dry season, W=wet season, and 3=2003, 4=2004, 5=2005; MT stands for the preliminary MTSAT fits.

	LW				SW	
	Land		Ocean		Land	Ocean
	Day	Nt	Day	Nt	Day	Day
D3	5.9	6.3	7.1	8.0	0.008	0.020
	2.0%	2.2%	2.6%	2.9%	4.8%	14.7%
W3	7.4	10.4	9.2	8.8	0.015	0.028
	2.9%	4.9%	3.9%	3.7%	6.8%	15.4%
D4	6.1	7.2	6.2	7.3	0.012	0.016
	2.1%	2.7%	2.3%	2.7%	6.1%	11.2%
W4	7.8	10.1	7.8	8.2	0.017	0.024
	3.0%	4.8%	3.3%	3.4%	7.5%	12.4%
D5	6.1	6.5	7.2	7.6	0.012	0.021
	2.1%	2.3%	2.7%	2.7%	6.4%	15.0%
MT	7.5	9.6	8.7	9.1	0.019	0.026
	2.8%	4.2%	3.6%	3.7%	8.9%	15.9%

In addition to accounting for seasonal and land/ocean differences, the TWP Darwin LW NB-BB fits strive to capture diurnal variability, by deriving separate fits for daytime and nighttime. Figure 3a shows LW daytime NB-BB regression fits for the wet season (Nov03-Apr04) over land around Darwin. For 1831 cases, the average daytime CERES BB LW flux is  $258.5 W/m^2$ , corresponding to an average GOES NB flux of  $51.6 W/m^2$ . The RMS error is 2.9%.

For the nighttime ocean dry season (May-Oct04), the average CERES BB and GOES NB fluxes are  $269.5$  and  $50.2 W/m^2$ , respectively (Fig 3b). The RMS error, 2.7%, is slightly smaller than that for the daytime land wet season. LW regressions were also performed for both dry and wet seasons, land and ocean, and also day and night (not shown). The LW regression RMS errors are also listed in Table 1. The regression coefficients ( $A_x$ ) listed in each plot can be used to convert NB fluxes to BB, using equation (2) for LW. A third order correction is made to the data at nighttime, as well as ocean daytime, to reduce the low-end bias evident in Fig. 3.

These NB-BB fits are assessed to determine if there are any flux-dependent biases by comparing the CERES and NB-derived fluxes for the data used in deriving the fits. Figure 4 shows the CERES and VISST-derived SW BB fluxes for (a) GOES-9 during the entire period May03-Oct05 and (b) MTSAT during Oct-Dec07. The biases are  $0.20$  and  $-0.20 W/m^2$ , for the respective datasets. Since the seasonal coefficients were derived using *Terra*, these SW NB-BB fits compare well at *Terra* overpass times. However, due to *Terra's* limited overpasses, these GOES-*Terra* NB-BB fits may not do as well at capturing the diurnal variability. To assess accuracy at other times, GOES-derived BB fluxes were also compared to *Aqua* (1330-LT crossing time) CERES data from the same time period for a  $2^\circ$  region ( $12^\circ-14^\circ S$ ,  $130.5^\circ-131.5^\circ E$ ) near the Darwin site (not shown). The bias is  $7.5 W/m^2$  and RMS error is  $26.3 W/m^2$ . Some of the bias may be due to differences between the *Terra* and *Aqua* CERES SW calibrations.

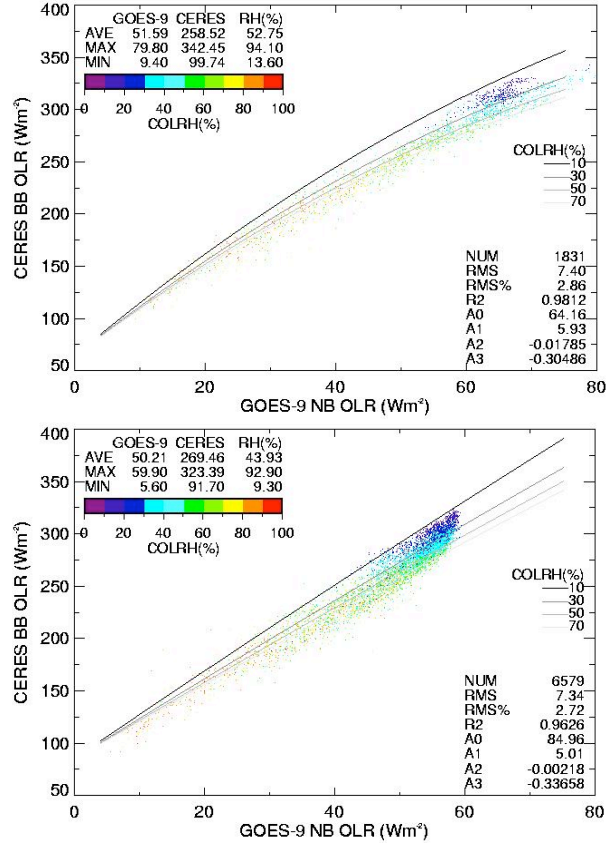


**Fig. 3.** Regression of GOES LW NB and Terra CERES BB fluxes over the Darwin region: (a) daytime Wet03 land cases and (b) nighttime Dry04 ocean cases. The NB-BB coefficients ( $A_x$ ) are listed at the lower right of each plot.

Figure 5 shows the VISST-derived LW BB fluxes compared with their CERES counterparts for (a) GOES-9 during the entire period May03-Oct05 and (b) MTSAT during Oct-Dec07. The respective biases are  $0.5$  and  $1.0 W/m^2$ . Since the seasonal coefficients were derived using *Terra*, it is expected that these LW NB-BB fits compare well at *Terra* overpass times. The LW fluxes were computed for GOES-9 data and matched with those from CERES aboard *Aqua*. The LW *Aqua* comparison (not shown) yielded a bias of  $-2.5 W/m^2$  and RMS error of  $11.3 W/m^2$ . Again, part of the bias may be due to *Aqua-Terra* differences in the *Aqua* and *Terra* calibrations. Also, the number of *Aqua* samples is much smaller than seen for the *Terra* comparisons.

#### 4. DISCUSSION

Comparisons of the seasonal VISST-derived BB fluxes with CERES observed BB fluxes show the updated fits agree well at *Terra* overpass times but have some departures from CERES with *Aqua* 3 hours later. However, this is a very limited validation. In order to further gauge the effects of these new fits on the derivation of BB fluxes, the data need to be evaluated throughout the diurnal cycle. BB fluxes derived using the Fu-Liou radiative transfer model are used to examine the diurnal variation of the NB-estimated BB fluxes.

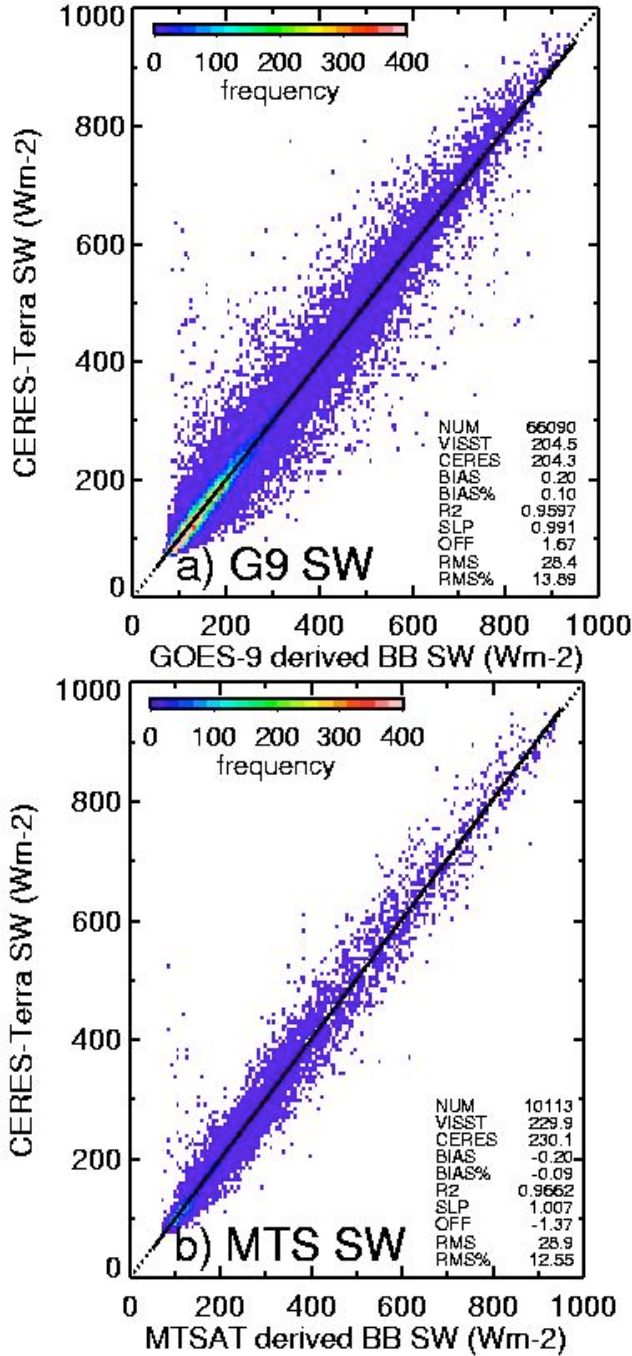


**Fig. 4.** Comparison of SW CERES BB fluxes (y-axis) and VISST BB fluxes (x-axis) derived using updated seasonal/land/ocean NB-BB fits for a) GOES-9 and b) MTSAT.

Figure 6 shows a scatterplot of clear-sky VISST-derived BB SW fluxes (y-axis) versus Fu-Liou (x-axis) derived for May-Oct03 dry season, for a 1° box centered inland near Darwin at 13.5°S 131°E. Clear-sky data is defined as any data where the VISST-derived cloud amount is < 5%, and the data is limited to SZA < 80°. The bias is only -0.36%; however, the comparison shows a departure from the one-to-one agreement line,

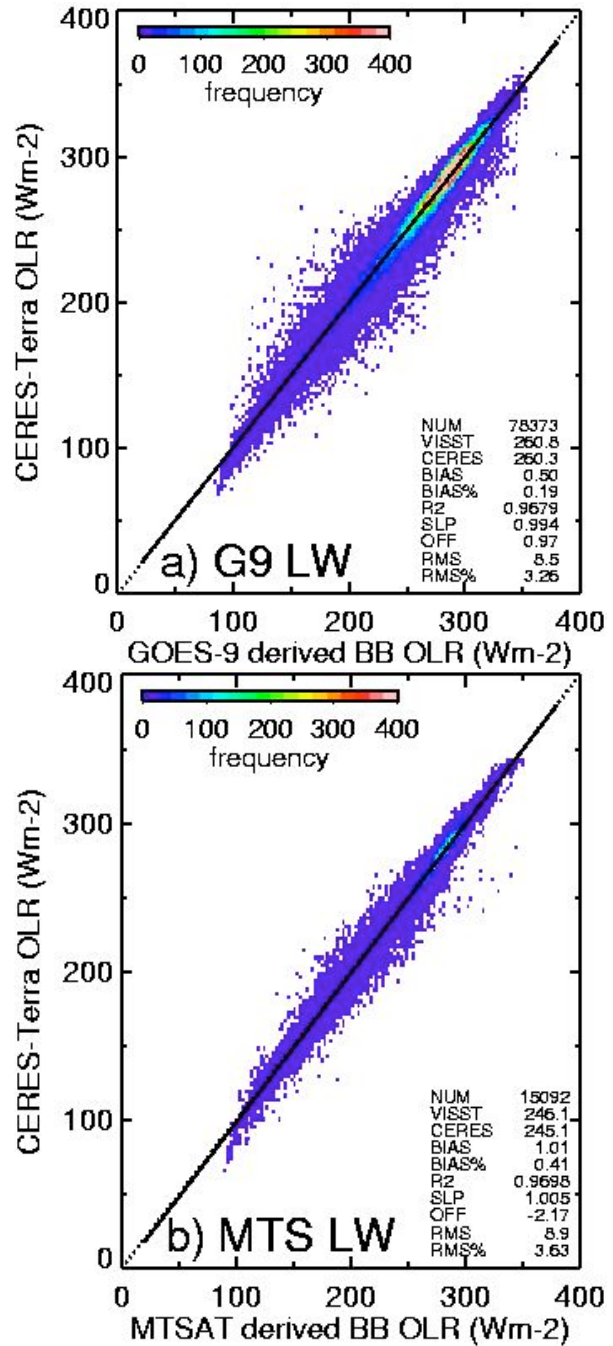


**Fig. 5.** Comparison of LW CERES BB fluxes (y-axis) and derived BB fluxes (x-axis) derived using updated seasonal/day/night NB-BB fits for a) GOES9 and b) MTSAT.

with a slope of 0.81. Comparisons of VISST-derived BB SW albedos were performed for all seasons from Oct03-Apr05; the bias and standard deviations of each month are summarized in Table 2.

To examine errors in the VISST-derived BB SW albedos with time, half-hour binned averages of the data shown in Fig. 6 are compared with Fu-Liou throughout the day (Fig. 7). The red curve shows the diurnal curve

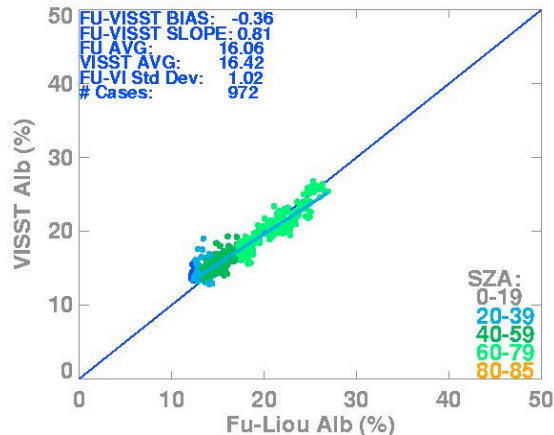


**Fig. 6.** Comparison of clear-sky Fu-Liou-derived SW BB albedos (x-axis) with GOES9 VISST-derived (y-axis) fit, for May-Oct03 dry season.

of SW BB albedos derived from the GOES-9 fit and the blue shows the Fu-Liou-derived clear-sky BB albedos. Compared to the theoretical results, the Dry03 VISST fit yields a realistic diurnal cycle, although the amplitude is not as great as that of the computed fluxes. However, the BB albedos derived from the GOES-9 fits follow the Fu-Liou-derived albedos more closely later in the evening, and earlier in the morning. At the Terra and Aqua overpass times, the GOES-9 albedos are greater by 1 – 2%. Since those are the times when the fits were developed and there appears to be no bias at low (clear) of the range in Fig. 4, those should be the most accurate values of SW albedo determined from the GOES-9 data. Thus, the Fu-Liou curve may need to be shifted upward to account for any differences between the assumed surface albedo and the actual surface albedo for this particular region. If that were the case the differences would shift to the extreme hours of the day. In either case, the results provide a reasonably accurate depiction of the diurnal cycle of clear-sky albedo given the uncertainties in the surface albedo and its variation with SZA.

The updated seasonal/day/night LW fits are also evaluated with respect to the Fu-Liou calculations. Figure 8 shows the comparison of Wet04 (a) daytime-only VISST-derived BB LW fluxes and (b) day and night VISST-derived BB LW versus the theoretical results. The comparison between Fu-Liou and the daytime VISST shows a bias of  $5.4 \text{ W/m}^2$  that drops to  $-1.0 \text{ W/m}^2$  when the nighttime points are added. The slope is reasonable for both fits, at 0.88 for daytime only, and 0.86 for both night and daytime points. The LW biases are summarized, for both clear sky and all data, in Table 3. Despite the relatively small biases, on average, the differences are greater at the extremes of the data. These systematic differences could be due to a number of factors. At the high end of the range uncertainties in the surface emissivity and the actual skin temperature could cause some systematic biases. For example, if the emissivity were too large, the TOA LW flux computed with the model would be too great even if the skin temperature was perfect. If the skin temperature

**Table 2.** Summary of bias and standard deviations for differences in Fu-Liou derived and GOES9-derived clear-sky SW albedoes, by season.

	SW Fu-Liou – GOES-Derived	
	Clr Bias (%)	Std Dev
Dry03	-0.4	1.0
Wet03	-0.5	1.1
Dry04	-0.2	1.5
Wet04	-0.8	1.2

was systematically too high, it would produce overestimates of the LW flux at the TOA. At the low end of the range, the assumption that the cloud top height was the radiating center of the cloud could result in underestimating the LW flux. Fully understanding these differences will require additional analysis.

To examine the errors diurnally, the VISST-derived BB LW fluxes were averaged at each half hour and plotted in Fig. 9 for the Dry04 cases (top graphs) and the Wet04 cases (bottom graphs). For the Wet04 cases, the seasonal/day/night NB-BB fit VISST-derived fluxes track the Fu-Liou results fairly well. However, the fits seem to overpredict at night and underpredict during the day. The underprediction is greatest in the morning, and improves in the afternoon and early evening. This phenomena could be due to a terrain-related azimuthal effect. Dry04 data show good agreement at night, which may be due in part to offsetting biases in cloudy and clear sky data. Daytime Dry04 LW fluxes are not in as good agreement, which may be due to the use of the ECMWF/DAO skin temperatures in the Fu-Liou calculations. There is apparently a lag in the model skin temperatures compared the observations. The lag is not as evident during the wet season, probably because of the clouds dominating the fluxes. The Dry03 and Wet03 curves show similar trends (not shown).

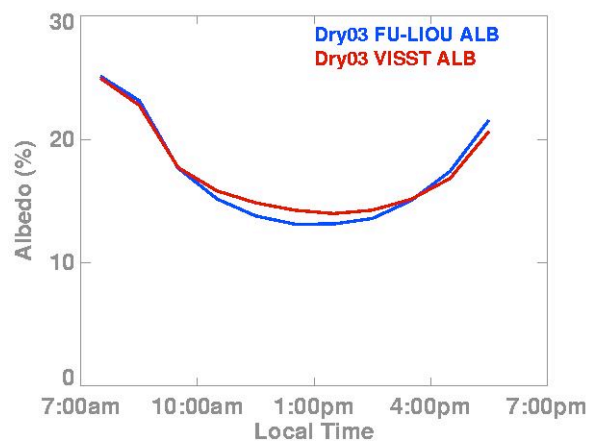


**Fig. 7.** Diurnal plot of half-hourly averaged BB SW clear-sky albedos derived using Fu-Liou radiative transfer code (blue) and VISST GOES9 seasonal fit (red), for a  $1^\circ$  box centered inland near Darwin.

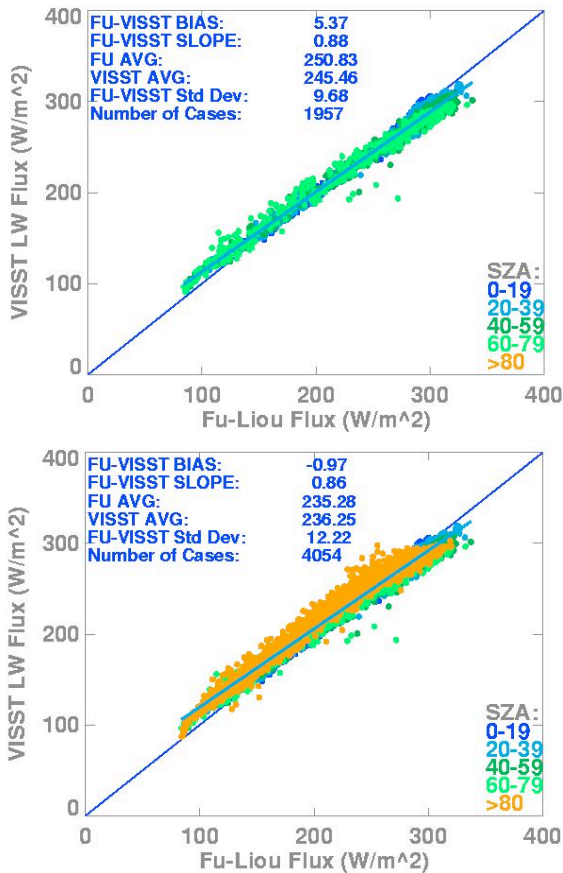


**Fig. 8.** Comparison of clear-sky LW Fu-Liou-derived BB LW flux (x-axis) versus VISST-derived BB LW flux (y-axis) for Wet04 season (a) daytime cases and (b) day and night cases.

### 5. SUMMARY AND FUTURE WORK

The seasonal LW and SW NB-BB fits show promise for yielding accurate VISST-derived BB fluxes. For the SW NB-BB fit, a realistic diurnal cycle was derived. Discrepancies with the Fu-Liou results during midday may be improved by adding the CERES data from *Aqua* overpasses at 1:30 pm local time, when deriving new NB-BB fits or using a more realistic surface albedo in the model calculations.

**Table 3.** Summary of bias and standard deviations for differences in Fu-Liou derived and GOES9/MTSAT-derived LW fluxes, by season; statistics are given for daytime only, as well as all points (night and day).

	LW (W/m <sup>2</sup> )			
	Clr Bias		Tot Bias	
	All	Day	All	Day
Dry03	2.1	-0.4	2.4	2.5
Wet03	5.6	5.5	-2.7	2.1
Dry04	1.2	-1.7	0.8	0.5
Wet04	8.0	8.4	-1.0	5.4
MTS	-1.2	-1.6	-4.3	2.4

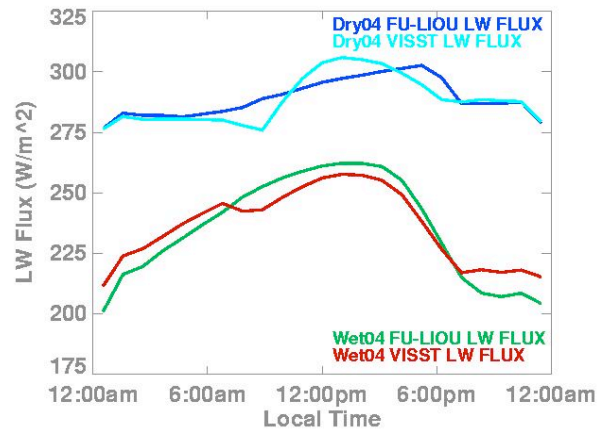


**Fig. 9** Diurnal plot of half-hourly averaged clear and cloudy BB LW fluxes for Dry03 Fu-Liou (dark blue), VISST fit (light blue), and Wet03 Fu-Liou (green), VISST fit (red).

The day/night/seasonal LW NB-BB fits provide reasonable BB LW fluxes. In addition to including *Aqua* overpass times into the derivation of NB-BB fits, future work includes a more rigorous correction to fully eliminate the low-end bias.

MTSAT1-R NB-BB fits will be derived for both wet and dry seasons. As this satellite has been replaced by MTSAT2-R as of July 2010, new NB-BB fits to account for the change will be derived.

### 6. ACKNOWLEDGEMENTS

This research was supported by the U.S. Department of Energy Interagency Agreement No. 18971 with NASA LaRC through Batelle, PNNL and Interagency Agreement DE-AI02-07ER64546.

### 7. REFERENCES

Geier, E.B., R. N. Green, D. P. Kratz, P. Minnis, W. F. Miller, S. K. Nolan, and C. B. Franklin, 2001: Single satellite footprint TOA/surface fluxes and clouds (SSF) collection document. [available on-line from [http://ceres.larc.nasa.gov/collect\\_guide.php](http://ceres.larc.nasa.gov/collect_guide.php).]

Fu, Q. and K. N. Liou, 1993: Parameterization of the radiative properties of cirrus clouds. *Journal of Atmospheric Sciences*, **50**, pp. 2008-2025

Khaiyer, M.M., P. Minnis, D.R. Doelling, M.L. Nordeen, R. Palikonda, and Y. Yi, 2009: Validation of Improved Broadband Shortwave and Longwave Fluxes Derived from GOES. *Proc. 16th Conference on Satellite Meteorology and Oceanography, Phoenix, AZ, Jan 11-15, 2009*

Loeb, N.G., N.M. Smith, S. Kato, W.F. Miller, S.K. Gupta, P. Minnis, and B. A. Wielicki, 2003: Angular distribution models for top-of-atmosphere radiative flux estimation from the Clouds and the Earth's Radiant Energy System instrument on the Tropical Rainfall Measuring Mission Satellite. Part I: Methodology, *J. Appl. Meteor.*, **42**, 240-265

Minnis, P., S. Sun-Mack, D. F. Young, P. W. Heck, D. P.

- Garber, Y. Chen, D. A. Spangenberg, R. F. Arduini, Q. Z. Trepte, W. L. Smith, Jr., J. K. Ayers, S. C. Gibson, W. F. Miller, V. Chakrapani, Y. Takano, K-N. Liou, Y. Xie, 2010: CERES Edition-2 cloud property retrievals using TRMM VIRS and Terra and Aqua MODIS data, Part I: Algorithms, Submitted to *IEEE Trans. Geosci. Remote Sens.*
- Rutan, D., F. Rose, M. Roman, N. Manalo-Smith, C. Schaaf, and T. Charlock (2009), Development and assessment of broadband surface albedo from Clouds and the Earth's Radiant Energy System Clouds and Radiation Swath data product, *J. Geophys. Res.*, 114, D08125, doi:10.1029/2008JD010669.
- Wielicki, B. A., et al., 1998: Clouds and the Earth's Radiant Energy System (CERES): Algorithm Overview. *IEEE Trans. Geosci. and Remote Sens.*, 36, 1127-1141.
- Wilber, A.C., D.P.Kratz, S.K.Gupta, 1999: Surface Emissivity Maps for Use in Satellite Retrievals of Longwave Radiation. NASA/TP-1999-209362, 35 pp.